

The BeppoSAX High Energy Large Area Survey HELLAS, II: Number counts and X-ray spectral properties

F. Fiore^{1,2,3}, P. Giommi¹, C. Vignali^{4,5}, A. Comastri⁵, G. Matt⁶, G.C. Perola⁶,
F. La Franca⁶, S. Molendi⁷, F. Tamburelli¹, and L.A. Antonelli²

¹ *BeppoSAX Science Data Center, Via Corcolle 19, I-00131 Roma, Italy*

² *Osservatorio Astronomico di Roma, Via Frascati 33, I-00044 Monteporzio, Italy*

³ *Harvard-Smithsonian Center of Astrophysics, 60 Garden Street, Cambridge MA 02138 USA*

⁴ *Dipartimento di Astronomia, Università di Bologna, via Ranzani 1, I-40127 Bologna, Italy*

⁵ *Osservatorio Astronomico di Bologna, via Ranzani 1, I-40127 Bologna, Italy*

⁶ *Dipartimento di Fisica, Università degli Studi “Roma Tre”, Via della Vasca Navale 84, I-00146 Roma, Italy*

⁷ *IFCTR/CNR, via Bassini 15, Milano, I-20133, Italy*

1 February 2008

ABSTRACT

The BeppoSAX High Energy Large Area Survey (HELLAS) has surveyed about 85 deg² of sky in the 5–10 keV band down to a flux of $4 - 5 \times 10^{-14}$ erg cm⁻² s⁻¹. The source surface density of 16.9 ± 6.4 deg⁻² at the survey limit corresponds to a resolved fraction of the 5–10 keV X-ray background (XRB) of the order of 20–30 %.

Hardness ratios analysis indicates that the spectra of a substantial fraction of the HELLAS sources (at least one third) are harder than a $\alpha_E = 0.6$ power law. This hardness may be due to large absorbing columns. The hardness ratio analysis also indicates that many HELLAS sources may have a spectrum more complex than a single absorbed power law. A soft component, superimposed to a strongly cut-off power law, is likely to be present in several sources.

Key words: X-ray: selection – background – galaxies – AGN

1 INTRODUCTION

Hard X-ray observations are very efficient in tracing emission due to accretion mechanisms, like in Active Galactic Nuclei (AGN). Hard X-ray selection is not affected by strong biases present at other wavelengths. For example, a column of a few times 10^{22} cm⁻² has negligible effect in the 5–10 keV band, while it reduces by ~ 100 times nuclear emission below 2 keV. Optical and UV color selection is biased against objects with even modest extinction or an intrinsically ‘red’ emission spectrum (see e.g. Vignali et al. 2000, Maiolino et al. 2000). However, the space density and evolutionary properties of the hard X-ray sources are still basically unknown. We therefore decided to take advantage of the large field of view and relatively high sensitivity and spatial resolution of the BeppoSAX MECS (Boella et al. 1997a,b) to perform a large area survey in the hardest band (5–10 keV) which is reachable so far with imaging instruments. Chandra and XMM-Newton go much deeper than BeppoSAX at low energies, but in the 5–10 keV band the BeppoSAX MECS collecting area is comparable to that of Chandra ACIS and it is a factor of 5–10 smaller than that of

XMM-Newton Epic PN. However, the MECS field of view is a factor of about 7 larger than that of the Chandra ACIS-I instrument and about 3 times larger than that of the XMM Epic PN. Therefore, these instruments will cover, at least for the first few years of operations, a relatively small portion of the sky. The BeppoSAX shallower but larger area survey nicely complements deep pencil beam *Chandra* and XMM-*Newton* surveys (Mushotzky et al. 2000, Giacconi et al. 2001, Hasinger et al. 2001, Hornschemeier et al. 2001). The main scientific purpose of the BeppoSAX MECS survey is therefore to study the nature of the hard X-ray source population and in particular to provide a relatively large sample of sources bright enough to measure, with the present generation of X-ray satellites, their main X-ray spectral properties. This will allow for the first time the statistical study of the distribution and evolution of the obscuring gas in a hard X-ray selected sample.

Preliminary results on this survey have been presented by Giommi et al. (1998), Ricci et al. (1998), Comastri et al. (1999, 2000), Matt et al. (1998), Fiore et al. (1998, 2000). These indicate that the BeppoSAX survey has resolved 20 to 30% of the hard XRB and that the large majority of the

sources so far identified are AGN in agreement with optical identifications results of ASCA surveys in the 2–10 keV energy range (Akiyama et al. 2000). Interestingly enough the fraction of obscured AGN among the about 70 optically identified HELLAS sources is higher than in the ROSAT and ASCA samples (Fiore et al. 1999, Fiore et al. 2000, La Franca et al. in preparation).

In this paper we present the survey and discuss the sources X-ray spectral properties. An analysis of the BeppoSAX MECS position reconstruction accuracy is presented in the Appendix. A companion paper (Comastri et al. 2001) compares the observed number counts and absorbing column density distribution with AGN synthesis models for the hard X-ray cosmic background (XRB).

2 THE BEPPoSAX HELLAS SURVEY

The High Energy Large Area Survey (HELLAS) has been performed in the hard 4.5–10 keV, ‘octave’ wide, band for three reasons: a) this is the band closest to the maximum of the XRB energy density which is reachable with the current imaging X-ray telescopes; b) the BeppoSAX MECS (Boella et al. 1997b) Point Spread Function (PSF) greatly improves with energy: in the 4.5–10 keV band it is a factor of ~ 2 sharper than in the softer 1.5–4.5 keV band (providing a 95 % error radius of $1'$, see the Appendix and Ricci et al 1998), which allows optical identification of the sources; c) the MECS background (on-axis, internal + 70% Cosmic X-ray background) is $\sim 4.3 \times 10^{-3}$ counts s^{-1} arcmin $^{-2}$ (3 MECS units) in the 4.5–10 keV band and $\sim 3.0 \times 10^{-3}$ counts s^{-1} arcmin $^{-2}$ in the 1.3–4.5 keV band. So using the higher energy band only, reduces the total background by $\approx 40\%$, enhancing the chance of detecting faint, highly obscured or very hard sources, with few counts below 4.5 keV.

About 85 square degrees of sky have been surveyed in the 4.5–10 keV band using 142 BeppoSAX MECS high Galactic latitude ($|b| > 20$ deg) fields. There is no overlap among the fields and, wherever possible, multiple observations of the same field have been merged in one single pointing to increase the sensitivity. Fields were selected among public data (as March 1999) and our proprietary data. Fields centered on bright extended sources and bright Galactic sources were excluded from the survey, as well as fields close to LMC, SMC and M33. Most of the fields have exposures between 30 and 100 ks, and 20 fields have an exposure higher than 80 ks (Fig. 1).

2.1 Source detection

Coadded, sky coordinates MECS1+MECS2+MECS3 images (or MECS2+MECS3 images after the loss of MECS1 on May 7th 1997) have been analysed. Sources were detected in images accumulated between 4.5 and 10 keV. The lower limit is chosen to include in the band the Xenon L edges (the MECS Energy-PI relationship is non-linear across the edge). Cleaned and linearized MECS event files in the BeppoSAX SDC on line archive have always been used in this analysis. The reader is referred to the SDC on-line documentation and to Fiore, Guainazzi & Grandi (1999) for details on data reduction.

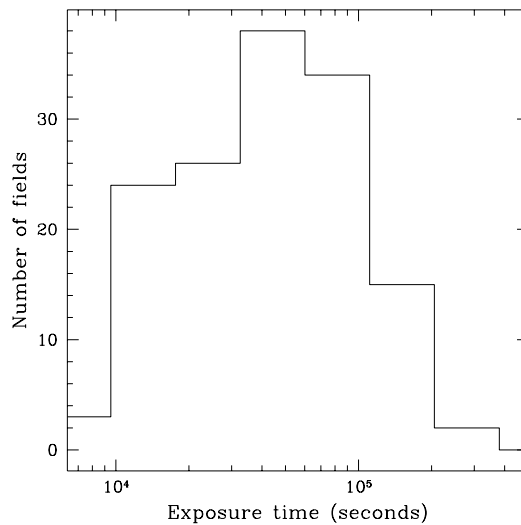


Figure 1. The distribution of the net exposure times in the 142 HELLAS fields.

We have used a variation of the DETECT routine included in the XIMAGE package (Giommi et al. 1991) to detect the X-ray sources. The method consists in first convolving the X-ray image with a wavelet function, to smooth the image and increase contrast, and then in running a standard slide-cell detection method on the smoothed image, to locate count excesses above the local background. The detection algorithm has been run several times for each field, changing the size of the slide-cell and the width of the wavelet function to take into account the variation of the MECS PSF with the off-axis angle, and to improve the efficiency in detecting extended sources. The quality of the detection has always been checked interactively. In particular, sources near the MECS Fe⁵⁵ calibration sources have been carefully tested for reliability running the detection algorithm after excluding a narrow energy interval centered on the iron feature at 5.894 keV. The final net counts are estimated from the original (un-smoothed) image, to preserve Poisson statistics. The background is calculated using ten source-free boxes near the source region and is rescaled at the source position to take into account the spatial variations of the MECS background (see the BeppoSAX SDC on line “cookbook”, <http://www.asdc.asi.it/bepposax/software/cookbook>, and Chiappetti et al. 1998). 175 sources have been detected in the 4.5–10 keV images with a probability higher than 99.94 % that they are not Poisson fluctuation of the background (after excluding the targets of the observations). The analysis of the 2–10 keV images is reported by Giommi, Perri & Fiore (2000).

2.2 Count rates and fluxes

Source count rates in four bands (1.3–10 keV, total, T, 1.3–2.5 keV, low band, L, 2.5–4.5 keV, middle band, M, and 4.5–10 keV, high band, H) were extracted and corrected for the energy dependent vignetting (as calibrated in orbit us-

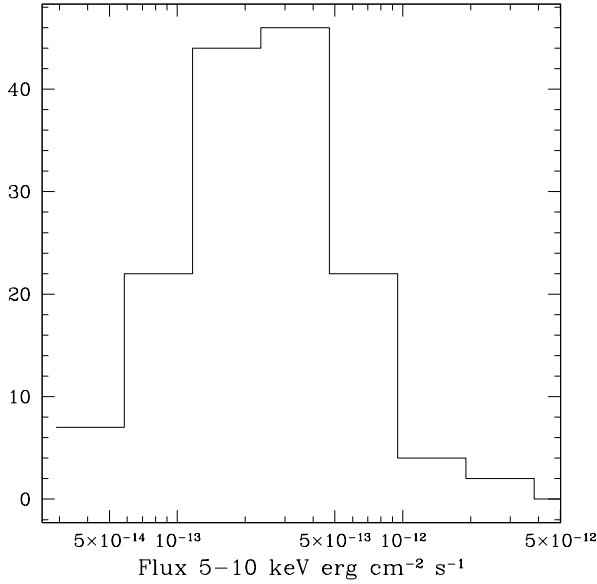


Figure 2. The histogram of the number of sources (non-target) detected as a function of the 5-10 keV flux.

ing a series of observations of the Crab nebula at different off-axis angles, Conti et al. 1997, Cusumano & Mineo 1998) and for the MECS PSF (using an analytical approximation of the PSF calibrated using observations of AGNs and Compact Galactic sources, Conti et al. 1997). The MECS 4.5-10 keV PSF half power radius is ~ 1.2 arcmin at off-axis angles ~ 7 arcmin, it increases to ~ 1.65 arcmin and ~ 2.2 arcmin at off-axis angles of 18.8 and 24.5 arcmin respectively. Even at these large off-axis angles the core can be safely considered axisymmetric. For faint sources ($S/N < 4$) all corrections were done at fixed energies, close to the mean energy for a power law spectrum with $\alpha_E = 0.6$ in the three bands L, M and H. For brighter sources the correction was done by convolving the vignetting and PSF functions with the source count histogram in the three L, M and H bands. The count rates were converted to fluxes using a conversion factor of 7.8×10^{-11} erg cm $^{-2}$ s $^{-1}$ (5-10 keV flux) per one “3 MECS count” (4.5-10 keV), appropriate for a power law spectrum with $\alpha_E = 0.6$. The factor is not strongly sensitive to the spectral shape, due to the narrow band: for $\alpha_E = 0.4$ and 0.8 it is 8.1 and 7.6×10^{-11} erg cm $^{-2}$ s $^{-1}$, respectively. A conversion factor of 9.9×10^{-11} erg cm $^{-2}$ s $^{-1}$ per one “3 MECS count” has been used for sources under the 550 micron Berillium strongback supporting the MECS window to account for the reduced detector sensitivity. The histogram of the number of sources as a function of the flux is given in figure 2.

2.3 Sky coverage

Figure 3a) gives, for the 175 *HELLAS* sources, the count rate as a function of the off-axis angle. The solid (dashed) model line represents the minimum detectable count rate (at the given threshold of 99.94 %) for an exposure time of

Table 1. *HELLAS* sky coverage and integral logN-logS

Flux 5-10 keV erg cm $^{-2}$ s $^{-1}$	sky coverage deg 2	logN-logS deg $^{-2}$
1.00×10^{-12}	84.2	0.0359 ± 0.0207 (0.035)
7.38×10^{-13}	77.1	0.0891 ± 0.0325 (0.070)
5.45×10^{-13}	67.7	0.253 ± 0.0579 (0.11)
4.02×10^{-13}	55.2	0.447 ± 0.0808 (0.21)
2.97×10^{-13}	37.5	0.952 ± 0.133 (0.32)
2.19×10^{-13}	25.2	1.54 ± 0.19 (0.42)
1.62×10^{-13}	15.9	2.40 ± 0.28 (0.68)
1.19×10^{-13}	8.3	4.43 ± 0.51 (1.1)
8.81×10^{-14}	4.7	5.92 ± 0.75 (2.2)
6.50×10^{-14}	2.9	10.3 ± 1.4 (2.8)
4.80×10^{-14}	0.75	16.9 ± 3.0 (6.4)

First quoted errors are the 1σ statistical confidence interval. Errors in brackets systematic uncertainties, see the text

100 ks in 3 (2) MECS units. These lines define the count rate limit (function of the exposure time and off axis angle) of the *HELLAS* survey. The shape of the model curves has been adjusted using the latest calibration of the telescope vignetting, MECS background and Berillium strongback. Their normalization has been chosen using extensive simulations. The survey has been simulated assuming a given logN-logS, a distribution of spectral shapes and the positions in detector coordinates of the *HELLAS* sources. The sky coverage of the simulated survey has been computed inverting the model curves. The normalization of the model curves (the on-axis flux limits for a 100 ks observation), and therefore the sky coverage, were then varied until the input logN-logS was correctly reproduced by the one computed from the simulations. The adopted value of the on-axis flux limit is $3 \times 10^{-14} (100/t(ks))^{0.5}$ erg cm $^{-2}$ s $^{-1}$ (3 MECS units). It is $5 \times 10^{-14} (100/t(ks))^{0.5}$ and $1.5 \times 10^{-13} (100/t(ks))^{0.5}$ at off-axis angles of 6 and 15 arcmin, respectively. Regions of radius 4, 6 or 8 arcmin around bright targets have been excluded from the sky coverage and sources detected in these regions have been excluded from the sample. The exclusion radius has been determined by imposing that the target count rate per square arcmin at a given off-axis radius is less than half of the local MECS background. Sources with a count rate smaller than the minimum value given by the model curves in figure 3a) normalized to the actual exposure time have also been excluded from the sample. This brings the total number of sources in the sample used for computing the logN-logS to **147**. The *HELLAS* source catalogue including the source identification number, the J2000.0 coordinates, the 5-10 keV flux and signal to noise and the count ratios in different energy ranges is reported in Table 2. The sky coverage computed assuming a power law spectrum with $\alpha_E = 0.6$ is given in figure 3b), thick solid line, and in table 1.

2.4 Spurious sources

Given a detection probability threshold P the number of spurious sources can be estimated by multiplying $(1-P)$ for the number of independent cells in the sky covered near a given flux limit. Faint fluxes ($F_X = 5 - 7 \times 10^{-14}$ erg cm $^{-2}$ s $^{-1}$

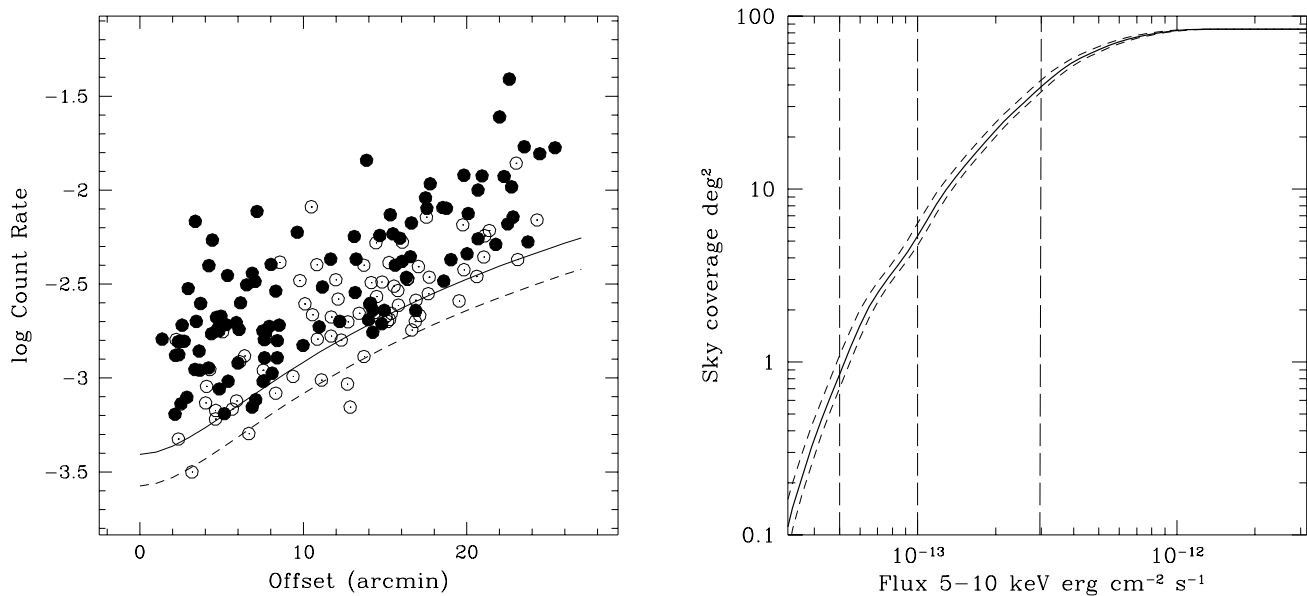


Figure 3. a) The MECS count rate as a function of the off-axis angle. Solid points are from observations with 3 MECS units, open points from observations with 2 MECS units. The solid (dashed) model line represents the minimum count rate detectable (at the given threshold of 99.94 %) for an exposure time of 100 ks in 3 (2) MECS units. b) The HELLAS sky coverage for three different models of the source spectrum: a power law with energy index of 0.6 (thick solid line), 0.2 and 1.0 (lower and upper dashed lines).

) can be probed only in the MECS inner < 8 arcmin, where the typical detection cell is of $0.004\text{--}0.005 \text{ deg}^2$. The skycoverage at these fluxes is of 1-3 degrees and therefore the number of faint spurious sources should be < 0.6 . Sources of flux of $3\text{--}10 \times 10^{-13} \text{ erg cm}^{-2} \text{ s}^{-1}$ can be detected in the whole MECS, with typical detection cells of $0.007\text{--}0.012 \text{ deg}^2$. The skycoverage at these fluxes is of 40 and 80 deg^2 and therefore, the number of spurious sources should be between 2.5 and 3.5. In total the fraction of spurious sources should be smaller than 5%. These numbers have been checked using simulations.

2.5 Flux and sky coverage uncertainties

The MECS absolute flux calibration has been obtained using several observation of the Crab nebula in the three years of the BeppoSAX mission. Assuming a power-law model the energy index and the 2-10 keV flux are found to be $\alpha_E = 1.088 \pm 0.002$ and $F_{2-10\text{keV}} = 2.008 \pm 0.006 \times 10^{-8} \text{ erg cm}^{-2} \text{ s}^{-1}$. Repeated observations have not revealed any significant variations in these parameters so far (Sacco 1999). Main flux and sky coverage uncertainties are due to the unknown spectrum of the sources near the detection limit. We evaluated this uncertainty by calculating fluxes and sky coverage in the two limiting cases of power law spectra with $\alpha_E = 0.2$ and 1.0 , see figure 3b, in addition to the default case (power law spectrum with $\alpha_E = 0.6$).

2.6 Source confusion

Source confusion is likely to affect surveys performed with instruments with limited spatial resolution like the Bep-

poSAX MECS. It is therefore important to quantify the effect of source confusion for the present survey. At 5-10 keV fluxes of $2.5\text{--}5\text{--}10 \times 10^{-14} \text{ erg cm}^{-2} \text{ s}^{-1}$ we expect less than 60, 20 and 7 sources per square degree, respectively, based on ASCA and BeppoSAX 2-10 keV surveys (e.g. Cagnoni et al. 1998, Ueda et al. 1998, Giommi et al. 2000). The probability to find two sources with comparable fluxes equal to the above values within 2-4 arcmin (twice the size of the typical slide-cells, see section 2.1) is $\sim 0.4\%$, $\sim 0.05\%$ and $\sim 3\%$ respectively. The fraction of confused sources with flux $\lesssim 1\text{--}2 \times 10^{-13} \text{ erg cm}^{-2} \text{ s}^{-1}$, should therefore be smaller than 10%. A comparison with the ROSAT PSPC may be instructive. The on-axis PSPC PSF is a factor of ≈ 3 sharper than the MECS one, but the source density at the PSPC flux limit for a 50 ks observation is 10-20 times higher than that at the HELLAS flux limit (see e.g. Zamorani et al. 1999), giving rise to similar confusion probabilities. Simulations confirmed the reliability of the above numbers.

We have also looked at the spatial extension and asymmetry in the counts distribution of the 147 sources to understand if any of these sources can be actually due to the contribution of 2 or more confused sources. We find that this might be the case for about 20 sources distributed in the whole range of fluxes. This is an upper limit to the number of confused sources, since some of these may of course be truly extended sources. In fact 6 of these sources have been already identified with clusters of galaxies. We will discuss this subsample more in detail in a follow-up publication. We conclude that confusion is likely to alter by little the results on the logN-logS presented in the next section.

2.7 The integral logN-logS

Figure 4 and table 1 present the integral 5-10 keV logN-logS of the 147 *HELLAS* sources. First quoted errors in Table 1 and solid error bars in figure 4 are the 1σ statistical confidence interval. Errors in brackets and dashed error bars in figure include systematic uncertainties, mainly due to the lack of knowledge of the real spectrum of the faint sources, see previous section. We find $16.9 \pm 3.0(6.4)$ sources deg^{-2} at $F_{5-10\text{keV}} = 4.8 \times 10^{-14} \text{ erg cm}^{-2} \text{ s}^{-1}$. This number corresponds to a resolved fraction of the 5-10 XRB equal to 20-30 %, depending on the XRB normalization (see Comastri 2000 and Vecchi et al. 1999).

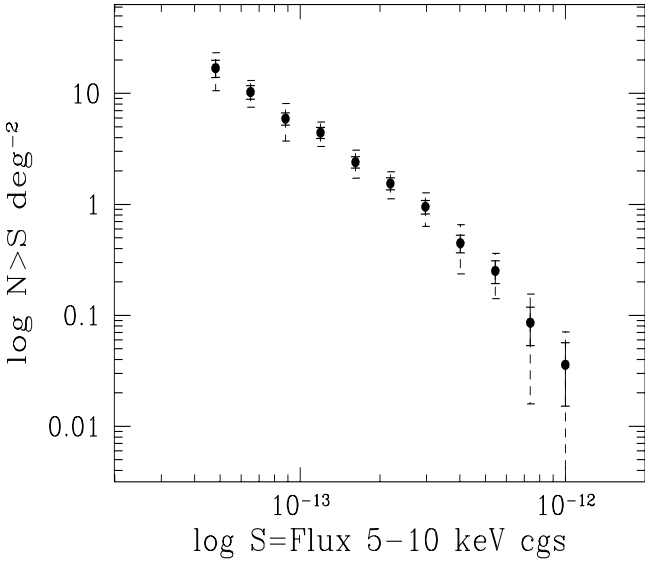


Figure 4. *HELLAS* 5-10 keV integral logN-logS. Solid error bars = 1σ statistical confidence interval. Dashed error bars include systematic uncertainties, see text.

3 X-RAY SPECTRAL ANALYSIS

For many of the *HELLAS* sources the total number of counts detected is <100 , preventing the use of proper spectral fitting procedures to study their spectrum. The broad band X-ray spectral properties of the *HELLAS* sources can however be investigated using count ratios. We have calculated for each source the softness ratio $(L+M-H)/(L+M+H)$, or $(S-H)/(S+H)$ ($L=1.3-2.5$ keV band, $M=2.5-4.5$ keV band, $S=L+M=1.3-4.5$ keV band, $H=4.5-10$ keV band), and the hardness ratios $\text{HR1}=(M-L)/(M+L)$ and $\text{HR2}=(H-M)/(H+M)$. MECS1 had a lower sensitivity at low energy ($E < 4$ keV) than MECS 2 and 3, because of a thicker Kapton filter. Therefore count ratios of sources observed with 3 MECS units have been corrected for this effect. The correction is however small, always smaller than the statistical errors. Sources under or close to the berillium strongback supporting the MECS window have been excluded from this

analysis, because their observed hardness may be systematically higher than real. The number of the remaining sources in the sample used for the following analysis is of 128. $(S-H)/(S+H)$ for these sources is given in Table 2. Figure 5 plots $(S-H)/(S+H)$ as a function of the source 5-10 keV flux. Many of the *HELLAS* sources have a low $(S-H)/(S+H)$, indicating a hard spectrum. Errors are however quite large. To evaluate the number of sources with a softness ratio inconsistent with that expected by an unobscured power law at a given confidence level, we have compared the counts observed in the 1.3-4.5 keV band with that predicted by a power law model, based on the 4.5-10 keV count rates. Assuming $\alpha_E = 0.6$, we find that 36 of the 128 sources have 1.3-4.5 keV count rates lower than that expected at confidence level $\gtrsim 95\%$. Five sources have low band count rates lower than expected at a confidence level $\gtrsim 99.7\%$. Large absorbing columns densities are likely responsible for the hard spectrum of these sources.

Most of these very hard sources have flux higher than $1 - 2 \times 10^{-13} \text{ erg cm}^{-2} \text{ s}^{-1}$. Indeed, a deficit of very hard sources at lower fluxes is evident in figure 5. There is a possible astrophysical reason for this deficit, namely a redshift effect: the observed softness ratio of sources with similar intrinsic absorbing column density increases with the redshift, as the observed cut-off energy moves toward lower energies. On the other hand, a deficit of faint hard sources can also be the result of a reduced sensitivity to hard sources. This is due to the rapid increase of the vignetting of the telescopes with the energy and with the off-axis angle. In other words, the sky coverage decreases faster for the hardest sources than for the softest ones. To quantify this effect we have computed loci of equal 4.5-10 keV count rate for a given flux, shown by dashed lines in figure 5. The strong curvature of these lines toward low values of $(S-H)/(S+H)$ indicate that most of the deficit of faint hard sources is probably due to this effect. The curves are bent toward high flux values at high $(S-H)/(S+H)$ too, because the MECS sensitivity is reduced for very soft sources by the berillium window, which absorbs most photons below ~ 2 keV. The 4.5-10 keV sensitivity is maximum for an unabsorbed power law spectrum of $\alpha_E = 0.6 - 0.8$.

Different symbols in figure 5 mark optically identified sources (Fiore et al. 1999, 2001, La Franca et al. 2001, in preparation). Note as several of the narrow line AGN and emission line galaxies have an hard X-ray, possibly absorbed, spectrum. Intriguingly, also some of the broad line AGN have an hard X-ray spectrum suggesting some absorption also in these sources. See Fiore et al. 2001 and Comastri et al. 2001 for a more detailed discussion.

The source spectra are likely to be more complex than a simple absorbed power law. To study in more detail this complexity we have computed the hardness ratios HR1 and HR2, plotted one against the other in figure 6. In this plot the analysis is limited to the 56 source with signal to noise > 3.8 (31 identified), not covered by the MECS strongback. Most of the points lie to the left of dashed and first solid line in figure, (absorbed power law models), suggesting that while substantial columns ($\log N_H = 22-24$) are likely in the *HELLAS* sources, soft components spilling out below 3-5 keV are also common in the sample, making softer HR2. A partial covering model has been used to parameterize an absorbed spectrum with a soft component. The innermost

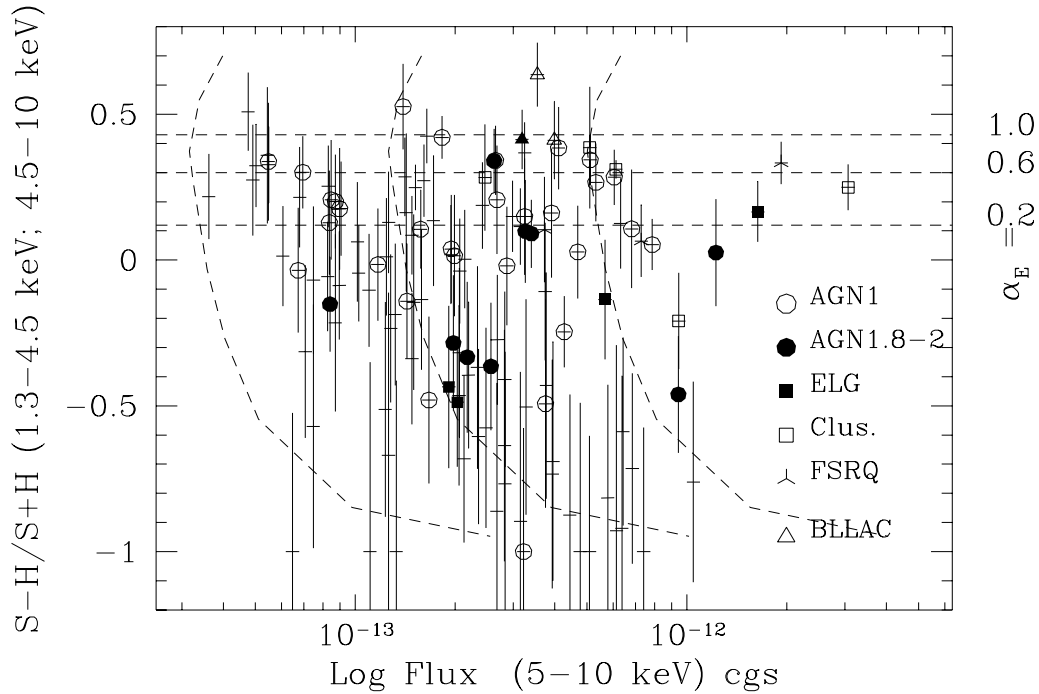


Figure 5. The softness ratio (S-H)/(S+H) plotted as a function of the 5-10 keV flux for the 128 sources in the HELLAS sample not partially or totally covered by the strongback support of the MECS window (57 optically identified sources). Different symbols mark identified sources: open circles = broad line quasars and Sy1; filled circles= type 1.8-1.9-2.0 AGN; filled squares= starburst galaxies and LINERS; open triangles= BL Lacertae objects; skeletal triangles= Broad Line Radio-loud quasars; filled triangles= radio galaxies; open squares= clusters of galaxies. Dashed lines mark loci of equal 4.5-10 keV count rate.

curve represents the expectation of such a model, with covering fraction of 90%. These models encompass most of the points, taking into account the rather large errors on the hardness ratios. The extreme position of the few points in the upper left part of the diagram is due to very few counts measured in the middle band, which makes extremely high HR2 and extremely low HR1. All these points are in any case consistent with the above mentioned simple models, within the errors. A more detailed analysis of the soft X-ray properties of the HELLAS sources is presented by Vignali et al. (2001) where the study of the X-ray spectrum is extended down to 0.5 keV using PSPC and HRI detections or upper limits.

4 DISCUSSION AND CONCLUSIONS

About 84 deg² of sky have been surveyed in the hard 5-10 keV band using 142 BeppoSAX MECS independent pointings. A statistically well defined and flux limited sample of 147 hard X-ray selected sources was assembled, and used to estimate the 5-10 keV logN-logS. The number counts are affected by both statistical and systematic errors. The latter, mainly due to the lack of knowledge on the spectrum of faint sources, have been estimated assuming a range of spectral slopes in the count rate to flux conversion. The source surface density ($\sim 16.9 \pm 6.4$ deg⁻²) at the survey flux limit of

4.8×10^{-14} erg cm⁻² s⁻¹ corresponds to a resolved fraction of the 5-10 keV XRB of the order of 20-30 % depending on the XRB normalization (Vecchi et al. 1999, Comastri 2000).

Hardness ratios have been used to study the X-ray spectrum of the HELLAS sources. These hardness ratios indicate rather hard spectra, harder than in previous 0.7-10 keV ASCA surveys (Ueda et al. 1999, Della Ceca et al. 1999). This hardness may be due to substantial absorbing columns. In fact, a large fraction of identified type 1.8-2 AGN show softness ratios similar to those expected from power law models reduced at low energy by column densities of log N_H =22-24, at the source redshift (see e.g. Fiore et al. 2000, 2001 and Comastri et al. 2001).

Many of the sources may have a softer component emerging below 3-4 keV. Indeed the cross-correlation between the HELLAS catalogue and the ROSAT PSPC public archive data (Vignali et al. 2001) indicates that about two third of the HELLAS sources in the field of view of a ROSAT observation have a counterpart in the soft (0.5-2 keV) energy range. The nature of such a component is still not clear and could be due to nuclear photons spilling from a partial covering screen or reflected from a warm-hot medium, or to extended extranuclear components, possibly related to circumnuclear starburst regions and winds. The presence of a soft component not directly related to the nuclear emission might easily lead to a wrong estimate of the intrinsic soft

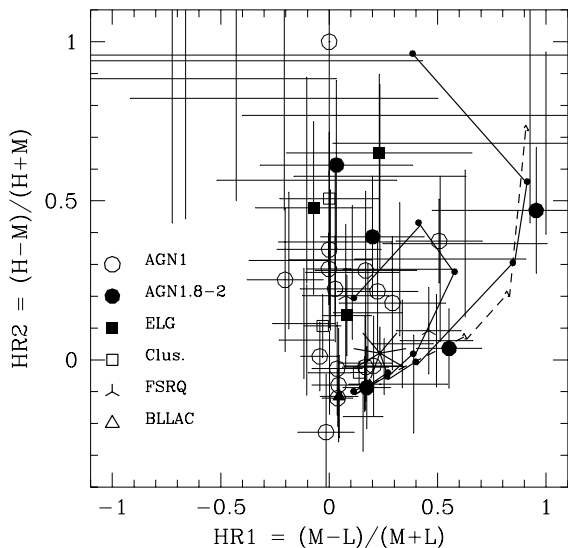


Figure 6. The hardness ratio $HR1=(M-L)/(M+L)$ as a function of the hardness ratio $HR2=(H-M)/(H+M)$ for the 56 sources not partially or totally covered by the strongback support of the MECS window and with signal to noise > 3.8 (32 optically identified sources). Symbols as in figure 5. The big star represent the predicted position for an unabsorbed power law source with $\alpha_E = 0.4$. The rightmost solid curve represents the expectation of a power law model with $\alpha_E = 0.8$ absorbed by a column of $\log N_H = 0, 22, 22.7, 23, 23.7$ and 24 (down to up) at $z=0$. The dashed curve represents the expectation of the same models with the absorber at $z=0.4$. The innermost solid curve represents the expectation of a partial covering model with $\log N_H$ as in the previous cases and covering fraction of 90%.

X-ray luminosity, especially for heavily absorbed sources. According with the XRB baseline model, absorbed AGN become progressively more important towards faint fluxes and thus spurious evolutionary terms can be introduced in the luminosity function derived from soft X-ray selected samples. An estimate of the importance of such a bias is not straightforward and also strongly model-dependent (see Miyaji et al. 2000 for a detailed discussion). The optical identification of a sizeable sample of hard X-ray selected sources coupled with more sensitive soft and hard X-ray surveys like those that will be performed in the near future by *Chandra* and *XMM-Newton* will provide new insights in this direction.

5 APPENDIX: POSITION ACCURACY

The location of an X-ray source by the BeppoSAX MECS is affected by statistical and systematical uncertainties.

The minimum number of counts in an *HELLAS* source is about 30, against about 100 backgrounds counts. For such faint sources, given the MECS PSF, the statistical uncertainty on the centroid is of 30-40 arcsec. For bright sources the uncertainty on the source centroid due to the PSF is

about 13 arcsec (1σ), measured using 12 observations of LMC X-3. On the other hands, systematic errors can often be larger than these figures. The main sources of systematic errors in BeppoSAX positions are:

- (i) The complete unavailability of the star-tracker “z” (the one co-aligned with the X-ray telescopes) in about 10 % of the observations. In these cases the error on the pointing position reconstruction can be as big as 2 arcmin.
- (ii) The unavailability of the star-tracker “z” for part of each orbit in most observations. This often produces “jumps” in the attitude reconstruction when passing control from one star-tracker to another. These “jumps” are due to a non perfect calibration of the misalignment between the three star-trackers. An error of about 20 arcsec in the on-board calibration of the misalignment has been discovered during summer 1997. It has been corrected in the on-board software at the beginning of May 1999. Observations performed after May 5th 1999 should provide more accurate positions than earlier observations.
- (iii) Since August 1997 BeppoSAX is operating in the so called “1 gyro mode”. For part of the orbit the satellite attitude is controlled by one star-tracker and one gyro. All configurations involving star-trackers “y” and “x” plus the gyro produce a pointing accuracy worse than the configurations including the star-trackers “y” and “x” simultaneously in the control loop, and those (the best) in which the star-tracker “z” is in the control loop.

Figure 7 shows the deviation in RA and Dec between the MECS sky positions and the optical (or radio) positions of a sample of 107 known AGN (targets or serendipitously found in the *HELLAS* fields). While the median deviation on dec is zero, MECS RA are systematically smaller than catalog ones by $\Delta RA \sim 15$ arcsec. The figure illustrates that when star-tracker “z” is not in the control loop the typical error on the position is between 1 and 1.5 arcmin. Sources detected at large off-axis angles show larger deviations because of the degradation of the MEVS PSF: the radii encompassing 67 % and 90 % of the 79 sources observed with z startracker in use and detected at off axis angle < 3 arcmin are 43 arcsec and 56 arcsec respectively. The same radii for the 19 sources detected at off-axis angles in the range 7-23 are 63 arcsec and 85 arcsec respectively.

Source positions in Table 2 were corrected for the above systematic effects by performing a simple boresight correction with respect to the known positions of the target and of any other known bright source in each field.

Acknowledgements

We thank the BeppoSAX SDC, SOC and OCC teams for the successful operation of the satellite and preliminary data reduction and screening, A. Matteuzzi for his work on MECS source position reconstruction, D. Ricci and M. Capalbi for the help with the BeppoSAX archive and databases. We also thank R. Maiolino, F. Pompilio, M. Perri, M. Salvati and G. Zamorani for useful discussions. This research has been partially supported by ASI contract ARS-99-75, MURST grants Cofin-98-032, Cofin-99-034, Cofin-00-02-36, and a 1999 CNAA grant.

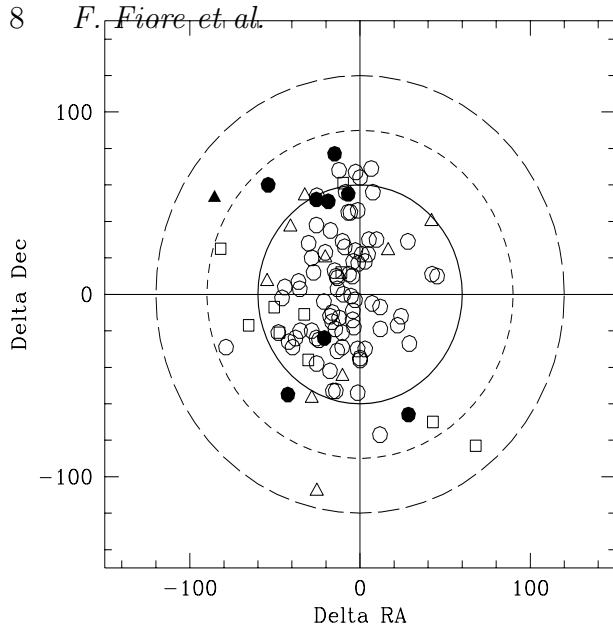


Figure 7. The deviation in RA and dec between the MECS position and the catalog position of 107 AGN (targets or serendipitously found in the fields) in the HELLAS survey. Filled symbols: sources observed without “z” startracker in the control loop. Open symbols: sources observed with “z” startracker for at least part of the time. Circles: sources detected at off-axis angles < 3 arcmin. Squares: sources detected at off-axis angles between 7 and 15 arcmin. Triangles: source detected outside 15 arcmin. The thick solid circle has a radius of 1 arcmin, the short-dashed and long-dashed circles have radii of 1.5 and 2 arcmin respectively.

REFERENCES

- Akiyama, M. et al. 2000, ApJ 532, 700
 Boella, G. et al. 1997a, A&AS, 122, 299
 Boella, G. et al. 1997b, A&AS, 122, 327
 Cagnoni, I., Della Ceca, R. & Maccacaro, T. 1998, ApJ, 493, 54
 Chiappetti, L. et al. 1998, Nuclear Physics B, (Proc. Suppl.), vol. 69/1, p.610
 Comastri, A., Fiore, F., Giommi, P., La Franca F., Elvis, M., Matt, G., Molendi, S., Perola, G.C., 1999, Adv. in Space Res., 25/3–4, 833
 Comastri, A., 2000, Astr. Lett. and Comm., in press, proceedings of the conference “X-ray Astronomy ’999, Stellar Endpoints, AGN and the Diffuse Background” (astro-ph/0003437)
 Comastri, A., Fiore, F., Vignali, C., La Franca, F. & Matt G. 2000, proceedings of the conference : “Large scale structure in the X-ray Universe” M. Plionis, I. Georgantopoulos eds. atlantisciences p. 227
 Comastri, A., Fiore, F., Vignali, C., Matt, G., Perola, G.C., La Franca F. 2001, MNRAS, in press
 Conti, G. et al. 1997, SPIE, 3113, 394
 Cusumano, G. & Mineo, T. 1998, ftp://www.sdc.asi.it/pub/sax/doc/reports/vignetting_rep.ps.gz
 Della Ceca, R., Castelli, G., Braitto, V., Cagnoni, I., & Maccacaro, T. 1999 ApJ, 524, 674
 Fiore, F. et al. 1998, proceedings of the first XMM workshop, ESTEC, October 1998, astro-ph/9811149
 Fiore, F., Guainazzi, M. & Grandi, P. 1999, Handbook for BeppoSAX NFI spectral analysis, ftp://www.sdc.asi.it/pub/sax/doc/software_docs/saxabc-v1.2.ps.gz
 Fiore, F. et al. 1999, MNRAS, 306, L55

- Fiore, F. et al. 2000, Astr. Lett. and Comm. in press, proceedings of the Bologna meeting “X-ray Astronomy ’999, Stellar Endpoints, AGN and the Diffuse Background” (astro-ph/0007118)
 Fiore, F. et. al. 2001, Proceedings of the ESO workshop on Deep Fields, (astro-ph/0102041)
 Giacconi R., Rosati P., Tozzi P., et al. 2000, ApJ in press (astro-ph/0007240)
 Giommi, P. et al. 1991, ApJ, 378, 77
 Giommi, P., Fiore, F., Ricci, D., Molendi, S., Maccarone, M.C. & Comastri, A. 1998, Nucl. Phys. B, 69/1-3, 591
 Giommi, P., Perri, M. & Fiore, F. 2000, A&A, 362, 799
 Hasinger, G. et al. 1998, A&A, 329, 482
 Hasinger, G. et al. 2001 A&A 365, L45
 Hornschemeier, A.E. et al. 2001, ApJ, in press, astro-ph/0101494
 Maiolino, R. et al. 2000, A&A, 355, L47
 Matt, G. 1998, proc. of the conference “High Energy Processes in accreting black holes”, astro-ph/9811053
 Miyaji, T., Hasinger, G. & Schmidt, M. 2000, A&A, 353, 25
 Mushotzky, R.F., Cowie L.L., Barger A.J., Arnaud K.A., 2000 Nature 404, 459
 Ricci, D., Fiore, F. & Giommi, P. 1998, Nucl. Phys. B, 69/1-3, 618
 Sacco B., in BeppoSAX June 1999 EIWG meeting report
 Ueda, Y. et al. 1998, Nature, 391, 866
 Ueda, Y. et al. 1999, ApJL, 524, L11
 Vecchi, A., Molendi, S. Guainazzi, M., Parmar, A. & Fiore F. 1999 A&A, 349, L73
 Vignali, C., Mignoli, M., Comastri, A., Maiolino, R. & Fiore, F. 2000, MNRAS 314, L11
 Vignali, C., Comastri, A., Fiore, F., La Franca, F. 2001, A&A, submitted
 Zamorani, G. et al. 1999, A&A, 346, 731

Table 2. *HELLAS* sample^a

RA (2000)	Dec (2000)	offset arcmin	Flux 5-10keV $10^{-13} \text{ erg cm}^{-2} \text{ s}^{-1}$	SNR	S-H/S+H	HR1	HR2	ID
0 26 36.5	-19 44 13	13.2	3.39	5.5	0.09 \pm 0.12	0.55 \pm 0.15	0.04 \pm 0.12	120
0 27 9.9	-19 26 31	6.2	1.83	6.5	0.42 \pm 0.07	0.04 \pm 0.07	-0.12 \pm 0.09	124
0 27 43.9	-19 30 29	11.0	1.58	3.4	-b-	-c-	-c-	121
0 45 49.6	-25 15 13	23.7	3.26	3.3	0.10 \pm 0.18	-c-	-c-	103.1
0 48 5.8	-25 4 32	14.9	1.48	3.6	-0.34 \pm 0.23	-c-	-c-	107
1 18 3.9	89 20 12	8.3	0.87	3.3	-0.21 \pm 0.30	-c-	-c-	431
1 21 56.8	-58 44 5	15.6	2.57	4.8	-0.36 \pm 0.22	0.03 \pm 0.35	0.61 \pm 0.27	39
1 34 14.3	-29 45 41	14.2	1.50	3.3	-0.14 \pm 0.30	-c-	-c-	99
1 34 28.6	-30 6 34	12.2	1.33	3.5	-b-	-c-	-c-	90
1 34 33.3	-29 58 38	6.0	0.87	3.9	0.20 \pm 0.16	-0.20 \pm 0.18	0.25 \pm 0.23	93
1 34 49.6	-30 2 34	5.4	0.71	3.5	-0.31 \pm 0.30	-c-	-c-	91
1 35 30.2	-29 51 21	8.4	0.90	3.2	0.18 \pm 0.21	-c-	-c-	96
1 40 8.9	-67 48 13	8.0	2.83	3.2	-0.41 \pm 0.30	-c-	-c-	20
1 53 3.9	89 12 20	2.4	0.54	3.1	0.36 \pm 0.23	-c-	-c-	426
2 42 1.8	0 0 46	10.0	1.47	3.7	-b-	-c-	-c-	172
2 42 9.4	0 2 29	7.5	0.68	3.2	0.22 \pm 0.17	-c-	-c-	174
3 8 8.5	89 8 41	4.9	0.65	3.5	-1.00 \pm 0.48	-c-	-c-	424
3 8 19.0	2 46 27	18.5	5.09	3.0	-1.00 \pm 0.40	-c-	-c-	195
3 15 45.0	-55 29 26	14.5	2.65	4.6	0.34 \pm 0.12	0.04 \pm 0.12	-0.03 \pm 0.15	45
3 17 32.4	-55 20 12	21.0	4.10	3.8	0.38 \pm 0.14	-c-	-c-	46
3 33 9.6	-36 19 40	15.2	3.98	3.3	0.41 \pm 0.13	-c-	-c-	72
3 34 7.4	-36 4 22	5.1	1.95	3.9	0.04 \pm 0.19	0.29 \pm 0.24	0.18 \pm 0.21	75
3 36 51.3	-36 15 57	14.7	3.72	3.9	0.10 \pm 0.18	0.08 \pm 0.20	0.20 \pm 0.22	73
4 32 27.9	5 13 5	15.0	2.06	3.3	-0.32 \pm 0.29	-c-	-c-	203
4 37 14.5	-47 30 58	16.0	2.68	3.5	0.21 \pm 0.19	-c-	-c-	53
4 38 47.9	-47 29 6	20.1	4.69	4.6	0.03 \pm 0.16	0.22 \pm 0.19	0.22 \pm 0.19	54
5 2 15.5	12 4 7	20.9	7.41	3.8	-1.00 \pm 0.43	-c-	-c-	220
5 15 13.7	1 8 7	7.6	1.26	3.3	0.13 \pm 0.17	-c-	-c-	185
5 20 48.3	-45 42 0	9.6	5.90	4.0	-b-	-b-	-b-	57
5 48 41.3	-60 52 18	19.5	2.42	3.4	0.19 \pm 0.15	-c-	-c-	32
5 50 0.2	-61 2 22	5.9	0.90	4.2	-0.09 \pm 0.19	0.33 \pm 0.26	0.28 \pm 0.21	26
5 52 6.1	-60 59 48	11.1	1.23	3.3	-b-	-c-	-c-	30
5 52 51.3	-60 57 18	17.1	2.06	3.9	-0.47 \pm 0.31	-0.66 \pm 0.70	0.88 \pm 0.44	31
6 23 56.6	-69 21 13	6.1	1.33	3.0	-1.00 \pm 0.59	-c-	-c-	6
6 25 31.3	-69 19 9	6.4	1.42	3.0	0.16 \pm 0.27	-c-	-c-	8
6 46 39.3	-44 15 35	16.6	4.27	6.9	-0.25 \pm 0.12	0.51 \pm 0.20	0.37 \pm 0.13	65
6 46 42.7	-44 32 29	19.0	2.68	4.0	-0.27 \pm 0.22	0.63 \pm 0.38	0.37 \pm 0.23	58
6 55 39.6	79 10 48	4.6	0.75	2.9	-0.57 \pm 0.42	-c-	-c-	405
7 21 29.6	71 14 4	8.1	0.84	3.5	0.13 \pm 0.18	-c-	-c-	385
7 41 40.3	74 14 57	22.6	30.66	7.5	0.25 \pm 0.08	-0.03 \pm 0.09	0.11 \pm 0.10	392
7 41 45.2	74 26 23	13.1	3.74	3.2	-0.11 \pm 0.24	-c-	-c-	393
7 43 9.1	74 29 19	7.2	6.05	6.3	0.28 \pm 0.09	0.17 \pm 0.11	-0.02 \pm 0.11	394
8 37 37.2	25 47 48	12.1	2.63	3.9	-b-	-b-	-b-	243
8 38 59.9	26 8 13	23.0	16.38	6.0	0.17 \pm 0.10	0.08 \pm 0.11	0.14 \pm 0.13	246
9 46 5.3	-14 2 59	15.8	2.82	3.8	-0.64 \pm 0.40	-c-	-c-	138
9 46 17.9	-14 10 27	10.9	2.04	3.5	-b-	-c-	-c-	136
9 46 32.8	-14 6 15	16.4	3.22	4.1	-1.00 \pm 0.42	-c-	1.00 \pm 0.42	137
10 29 19.1	50 48 15	17.5	5.78	3.0	-0.82 \pm 0.39	-c-	-c-	299
10 32 15.8	50 51 3	10.4	3.13	2.6	-b-	-c-	-c-	300
10 34 43.1	39 29 18	8.4	1.11	3.1	-1.00 \pm 0.65	-c-	-c-	273
10 34 52.0	39 40 12	5.3	1.41	4.4	0.29 \pm 0.13	-0.12 \pm 0.14	0.11 \pm 0.17	278
10 52 45.4	57 30 42	4.0	0.83	4.4	-0.06 \pm 0.19	0.03 \pm 0.26	0.37 \pm 0.23	321
10 54 19.8	57 25 9	13.4	2.62	5.0	0.34 \pm 0.11	0.17 \pm 0.11	-0.09 \pm 0.13	319
10 54 21.7	57 36 24	16.6	2.13	4.0	-0.68 \pm 0.29	1.00 \pm 0.98	0.68 \pm 0.29	323

Table 2. HELLAS sample^a

RA (2000)	Dec (2000)	offset arcmin	Flux 5-10keV 10^{-13} erg cm ⁻² s ⁻¹	SNR	S-H/S+H	HR1	HR2	ID
11 1 46.4	72 26 11	22.3	7.29	4.9	0.07 ±0.12	0.46±0.15	0.09±0.14	387
11 2 37.2	72 46 38	20.7	7.87	7.7	0.05 ±0.09	-0.00±0.10	0.29±0.11	390
11 6 14.0	72 43 16	8.5	1.67	3.6	-0.48 ±0.29	-c-	-c-	389
11 7 4.9	-18 16 28	7.7	1.23	3.1	-0.51 ±0.37	-c-	-c-	131
11 18 11.9	40 28 33	4.2	0.85	2.9	0.21 ±0.20	-c-	-c-	283
11 18 46.2	40 27 39	4.8	1.39	3.9	0.53 ±0.15	-0.01±0.13	-0.23±0.18	282
11 34 52.7	70 23 9	15.5	3.77	3.1	-0.43 ±0.39	-c-	-c-	380
11 56 39.2	65 17 57	5.7	0.75	3.2	-0.07 ±0.25	-c-	-c-	372
11 57 1.7	65 27 24	15.4	2.14	3.7	0.00 ±0.17	-c-	-c-	374
12 4 7.6	28 8 30	16.1	5.10	3.0	0.39 ±0.21	-c-	-c-	252
12 17 45.1	47 29 55	16.4	3.24	5.0	0.37 ±0.10	0.00±0.10	-0.04±0.13	292
12 17 50.3	30 7 8	19.8	3.54	3.2	0.64 ±0.11	-c-	-c-	265
12 18 55.0	29 58 12	12.7	1.98	3.3	-0.28 ±0.23	-c-	-c-	264
12 19 21.6	47 11 7	9.4	1.32	3.2	-b-	-c-	-c-	288
12 19 45.7	47 20 42	7.5	1.17	4.0	-0.02 ±0.19	0.00±0.24	0.35±0.25	290
12 22 6.8	75 26 17	6.5	2.46	3.5	0.28 ±0.18	-c-	-c-	400
12 29 23.7	1 51 38	14.1	1.61	4.3	0.27 ±0.12	0.17±0.12	-0.01±0.15	186
12 40 26.0	-5 13 20	11.7	3.13	4.3	-b-	0.17±0.16	0.10±0.17	167
12 40 29.6	-5 7 46	16.8	1.92	3.6	-0.44 ±0.28	-c-	-c-	169
12 54 28.0	59 21 1	24.3	6.37	2.9	-0.92 ±0.52	-c-	-c-	324
12 55 16.6	-5 39 22	16.3	2.20	4.0	-0.39 ±0.25	0.23±0.40	0.58±0.29	161
12 56 9.9	-5 54 30	7.6	0.91	3.6	0.18 ±0.16	-c-	-c-	157
13 4 24.3	-10 23 53	4.4	1.28	3.9	-0.23 ±0.25	-0.10±0.41	0.56±0.32	151
13 4 38.2	-10 15 47	5.9	1.43	3.8	-0.14 ±0.20	-c-	-c-	155
13 4 45.1	-5 33 37	7.5	1.26	3.0	-0.67 ±0.56	-c-	-c-	162
13 5 32.3	-10 32 35	22.0	19.27	7.2	0.33 ±0.07	0.16±0.07	-0.08±0.09	150
13 5 36.5	-5 43 30	22.7	6.42	3.4	-0.59 ±0.32	-c-	-c-	160
13 36 34.3	-33 57 47	21.8	3.18	4.6	0.41±0.10	0.05±0.09	-0.12±0.13	84
13 38 34.1	48 21 5	4.3	1.24	3.3	0.01 ±0.20	-c-	-c-	295
13 42 47.9	0 21 9	16.9	2.48	3.4	-0.58 ±0.34	-c-	-c-	180
13 42 59.3	0 1 38	20.6	3.25	3.2	0.15 ±0.20	-c-	-c-	176
13 48 20.8	-30 11 6	14.4	2.18	3.5	-0.33±0.26	-c-	-c-	100
13 48 24.3	-30 25 47	14.8	3.15	4.7	0.11±0.13	0.18±0.16	0.15±0.15	94
13 48 37.9	-30 9 11	12.3	1.59	3.2	-b-	-c-	-c-	101
13 48 45.4	-30 29 36	14.4	5.11	7.1	0.34±0.09	-0.04±0.09	0.01±0.11	92
13 50 9.4	-30 19 55	10.8	5.08	7.4	-b-	-b-	-b-	97
13 53 54.6	18 20 33	17.5	6.82	3.4	0.11 ±0.20	-c-	-c-	228
13 55 54.1	18 13 35	19.8	6.14	2.8	-0.93 ±0.64	-c-	-c-	226
14 11 58.7	-3 7 2	20.7	3.93	3.6	-0.73 ±0.39	-c-	-c-	171
14 17 12.5	24 59 28	12.9	0.69	3.7	0.30 ±0.12	-c-	-c-	239
14 18 31.1	25 11 7	8.6	6.11	18.7	0.31 ±0.03	0.14±0.03	-0.04±0.04	241
14 38 30.1	64 30 25	11.2	2.57	4.2	-b-	-b-	-b-	364
14 48 21.8	-69 20 30	11.7	4.25	5.0	-b-	-b-	-b-	10
15 19 39.9	65 35 46	13.9	9.43	5.2	-0.46 ±0.20	0.95±0.48	0.47±0.20	375
15 28 46.0	19 45 10	4.7	1.65	5.2	0.43 ±0.09	0.16±0.09	-0.18±0.11	230_2
15 28 47.3	19 39 10	5.0	1.57	5.3	0.11 ±0.13	0.03±0.16	0.22±0.17	230_1
16 26 56.8	55 13 24	14.2	3.15	3.1	-0.90 ±0.51	-c-	-c-	305
16 26 59.9	55 28 20	10.5	12.09	8.3				307
16 34 10.7	59 37 44	6.9	0.50	3.3	0.32 ±0.14	-c-	-c-	325
16 34 11.0	59 48 15	5.2	0.48	3.5	0.51 ±0.13	-c-	-c-	328
16 34 11.8	59 45 29	3.4	0.84	5.9	-0.15 ±0.16	0.20±0.24	0.39±0.19	327
16 49 57.9	4 53 32	19.8	9.45	5.0	-0.21 ±0.16	0.00±0.23	0.51±0.21	201
16 50 40.1	4 37 17	24.5	12.25	3.3	0.03 ±0.18	-c-	-c-	200
16 52 12.5	2 11 29	15.8	2.36	4.2	-0.60 ±0.30	-0.21±0.71	0.82±0.35	187
16 52 38.0	2 22 18	4.6	0.67	3.5	-0.04 ±0.21	-c-	-c-	190
16 54 41.1	40 2 10	17.6	6.32	4.1	0.13 ±0.16	-0.19±0.18	0.31±0.21	279

Table 2. *HELLAS* sample^a

RA (2000)	Dec (2000)	offset arcmin	Flux 5-10keV 10^{-13} erg cm ⁻² s ⁻¹	SNR	S-H/S+H	HR1	HR2	ID
17 40 10.7	67 42 50	17.7	3.28	3.0	-0.50 ±0.37	-c-	-c-	375.1
17 42 36.3	68 0 44	10.6	2.76	3.6	-b-	-c-	-c-	375.2
17 50 25.4	60 56 1	11.7	2.10	3.2	-b-	-c-	-c-	340.2
17 51 30.3	61 0 43	6.7	0.55	4.0	0.33 ±0.13	-0.10±0.13	0.06±0.17	346.2
17 52 38.3	61 5 47	3.2	0.36	3.3	0.22 ±0.15	-c-	-c-	351.1
17 53 49.0	60 59 52	12.7	1.10	3.8	-0.10 ±0.19	-c-	-c-	346.1
18 3 51.8	61 10 21	2.9	0.60	3.8	0.01 ±0.17	0.11±0.22	0.27±0.21	353
18 15 17.5	49 44 51	9.8	3.48	3.8	-b-	-b-	-b-	296
18 18 58.6	61 14 42	18.6	2.07	3.6	-0.04 ±0.18	-c-	-c-	354
18 19 18.4	60 56 6	3.5	1.52	8.1	0.25 ±0.08	0.25±0.09	-0.02±0.09	341
18 19 35.5	60 58 46	2.1	0.49	3.3	0.27 ±0.19	-c-	-c-	345
18 19 39.5	60 53 26	3.7	0.83	5.0	0.25 ±0.14	0.39±0.16	-0.08±0.15	337
18 36 11.3	-65 7 20	22.8	4.44	3.3	-0.88 ±0.41	-c-	-c-	25
20 42 47.6	-10 38 30	21.1	5.32	4.6	0.27±0.13	0.20±0.13	-0.02±0.16	147
20 44 34.8	-10 27 34	15.3	1.99	3.3	0.02±0.21	-c-	-c-	149
21 22 59.2	89 1 58	15.3	4.77	3.1	-1.00 ±0.51	-c-	-c-	413
21 38 8.9	-14 33 13	7.0	2.34	3.4	-0.37±0.35	-c-	-c-	134
21 42 46.7	89 35 30	23.5	10.47	4.2	-0.76 ±0.34	0.93±1.33	0.77±0.34	432
21 59 52.1	88 54 53	17.8	6.85	3.4	-0.72 ±0.33	-c-	-c-	410
22 3 0.5	-32 4 18	16.5	2.83	3.3	-0.77 ±0.45	-c-	-c-	85
22 26 30.3	21 11 56	13.7	3.91	2.9	0.16 ±0.22	-c-	-c-	237
22 31 49.6	11 32 8	15.2	1.94	4.2	0.02 ±0.17	0.01±0.19	0.31±0.22	213
22 41 22.1	29 42 41	15.6	2.98	5.0	0.15 ±0.12	0.34±0.14	0.05±0.14	256
22 42 51.5	29 35 32	7.6	1.02	3.6	-0.05 ±0.17	-c-	-c-	254
22 44 11.4	29 51 14	23.1	3.95	3.5	-0.69 ±0.41	-c-	-c-	258
23 2 30.1	8 37 6	17.6	2.67	3.9	-0.86 ±0.44	-0.43±2.64	0.96±0.46	206
23 2 36.2	8 56 42	10.1	3.17	5.2	-b-	-b-	-b-	212
23 6 59.2	8 48 40	4.1	1.02	3.0	0.06 ±0.20	-c-	-c-	210
23 15 36.4	-59 3 40	8.3	2.03	4.6	-0.49 ±0.22	0.23±0.43	0.65±0.25	37
23 16 9.8	-59 11 24	6.1	1.32	3.9	-0.19±0.24	0.51±0.39	0.32±0.26	35
23 19 22.1	-42 41 50	21.4	5.67	3.8	-0.14±0.20	-0.07±0.27	0.48±0.27	66
23 27 28.7	8 49 30	7.1	0.55	3.0	0.34 ±0.20	-c-	-c-	209
23 27 37.1	8 38 56	7.9	1.48	5.5	0.09 ±0.13	0.49±0.17	0.06±0.15	207
23 29 2.4	8 34 39	20.0	2.87	4.2	-0.02 ±0.20	0.17±0.23	0.28±0.25	205
23 31 55.6	19 38 34	17.0	3.75	3.0	-0.49 ±0.36	-c-	-c-	229
23 55 32.7	28 35 11	7.7	1.72	3.2	0.14 ±0.22	-c-	-c-	249
23 55 53.3	28 36 5	12.0	4.17	4.0	-b-	-b-	-b-	250

^a This table is also available at the following URL: <http://argos.mporzio.astro.it/hellas>^b partly obscured by the MECS strongback; -c- SNR < 3.8